ROYAL SOCIETY OF CHEMISTRY

PAPER

Check for updates

Recycling silicon photovoltaic cells into silicon anodes for Li-ion batteries using 3D printing†

Maryam Mottaghi, [ID] *[a] Apoorv Kulkarni [ID] [b] and Joshua M. Pearce [ID] [cd]

With the increasing adoption of solar energy, the disposal of end-of-life photovoltaic modules has become a growing environmental concern. As crystalline silicon has significant potential as an anode material for lithium-ion batteries, this study investigates recycling waste solar cell material into batteries using 3D printing. An open-source toolchain is developed to ensure accessible replication including a ball mill for grinding the waste silicon, a bottle roller for synthesizing novel stereolithography (SLA) resins and an SLA 3D printer for geometric control of the deposition of the materials. The materials were characterized at each step using spectrometry analysis, differential thermal analysis and thermogravimetric analysis of the polymer resin, optical microscopy on the printed parts, as well as scanning electron microscopy, energy-dispersive X-ray spectroscopy, and X-ray diffraction on the pyrolyzed parts. Electrochemical characterization, including cyclic voltammetry, galvanostatic charge–discharge, and electrochemical impedance spectroscopy, was performed on the assembled batteries. A mixture of 12% ground silicon solar cells with SLA resin was used for 3D printing the anodes and the samples were pyrolyzed at 1400 °C. The electrochemical tests from the anodes demonstrated a specific capacity of around 400 mA h g^{-1} with 89% capacity retention and coulombic efficiency more than 100% over 200 cycles. This study presents a promising sustainable solution by integrating recycled solar cell waste into lithium-ion battery anode production, which can address both waste management and energy storage challenges.

Sustainability spotlight

The growing amount of solar photovoltaic module waste poses significant environmental and economic concerns. This research addresses the challenge through fabrication of anodes for lithium-ion batteries through the recycling of silicon from discarded solar cells. Additionally, the integration of 3D printing techniques enables precise engineering of complex anode structures, enhancing battery performance by increasing energy density without sacrificing power density. This innovative approach represents a promising step toward improving the performance of sustainable and cost-effective energy storage devices as well as improving the end of life of photovoltaic systems. The batteries assembled with the recycled anode showed better performance than commercial graphite anode-based batteries showing the promise to provide lower cost batteries while enabling green end-of-use recycling for solar cells.

1 Introduction

Developing electronic devices such as portable electronics and electric vehicles and the demand for storing the green energy have attracted increasing interest and efforts toward investigating high performance energy storage devices among which electric batteries are designed to store and release electricity through electrochemical reactions.[1,2] Batteries are classified into primary (non-rechargeable, single-use) and secondary (rechargeable, reusable) types.[1] Rechargeable lithium-ion batteries dominate the secondary battery field due to their high theoretical charge capacity (4200 mA h g^{-1}), high energy density (300 W h kg^{-1}), and portability.[3–6] Lithium-ion batteries are made of three main parts: anode, cathode, and electrolyte. Graphite and carbon-based materials have been widely used as anodes due to the good electrochemical properties and low cost, but their applications are limited due to low capacity, which results in poor theoretical capacity in lithium ion batteries down to 372 mA h g^{-1}.[7,8] Silicon is one of the most promising alternatives for graphite due to its multiple advantages, including both abundance and a high specific capacity of about 3579 mA h g^{-1}.[8] Crystalline silicon (c-Si) photovoltaic (PV) modules, which make up over 93% of total production, contain about 0.67 kg of silicon per module which represent a significant source of silicon waste material.[9] Although PV is a well-established renewable energy source that provides a sustainable state[10] it still provides an operational life of 20–30 years

[a]Department of Mechanical and Materials Engineering, Western University, London, ON, Canada. E-mail: mmottagh@uwo.ca

[b]National Research Council, Ottawa, ON, Canada

[c]Department of Electrical & Computer Engineering, Western University, London, ON, Canada. E-mail: joshua.pearce@uwo.ca

[d]Ivey School of Business, Western University, London, ON, Canada

† Electronic supplementary information (ESI) available. See DOI: https://doi.org/10.1039/d4su00808a

under warranty.[11] At the end of 2016, there were around 250 000 metric tons of solar panel waste globally, and this volume is projected to increase to more than 60–78 million metric tons cumulatively by 2050.[11] Recycling this waste economically is a challenge[12,13] so establishing an upcycled application would have high value. Silicon in this solar waste is a good candidate for use in anodes in lithium-ion batteries because it has already undergone modification and purification.[14] Silicon-based anodes for large-scale applications are limited, however, due to their poor intrinsic conductivity, and huge volume change, more than 300%, during lithiation and de-lithiation. The volume change creates particle pulverization and repeated formation of solid electrolyte interface (SEI) layer that results in low coulombic efficiency (61.7%).[15–18] One of the solutions to address these issues is compositing silicon particles with carbon. In this regard, silicon provides the anode with high capacity while carbon increases the conductivity and alleviates the volume change by surrounding the silicon in the structure.[18] The conventional way to fabricate batteries is based on preparing slurries, then tape casting onto the current collector, and subsequently assembling and packaging the cell components.[19] Unfortunately, this fabrication method is difficult to optimize and customize the design and decreases the efficiency. For improving the energy density, a thicker anode is required to accommodate more active materials for storing Li ions inside the electrode, but through the conventional method, increasing the thickness is equal to decrease the power density since it is more difficult for the li ions to transport through the entire thickness and reach the active sited inside the structure.[20] To address this, 3D printing, with its ability to precisely control and engineer the design, can help achieve a shorter ion transportation distance while maintaining a high solid load of active materials. This approach allows for the enhancement of both energy density and power density simultaneously.[21] Various geometries have been proposed to enhance battery performance, among which the 3D porous structure is not achievable through conventional methods but can be easily fabricated using 3D printing. Among different 3D printing methods, direct ink writing (DIW), inkjet printing, photopolymerization, fused filament fabrication (FFF) (material extrusion), aerosol jet printing, and selective laser sintering are promising for battery fabrication.[22–24] Although the most popular 3D printing methods, the extrusion-based methods require complex material preparation to optimize the material rheological behaviour with high viscosity and suitable density.[25,26] Stereolithography (SLA), however, is not restricted by extrusion and provides the part with more flexibility, and design resolution comparing to other methods including FFF or DIW and can be a promising candidate for fabricating battery components. Thus, SLA printing of the Si based anode can be a solution to enhance the battery performance.[27] To test this hypothesis, in this work, a novel low-cost open-source hardware[28,29] method is proposed to 3D print the anode part of a Li-ion battery using silicon PV solar cell waste. For the first step, the waste is ground using an open-source ball mill to obtain <50 microns particles.[30] This particle size offers several advantages, including higher tapped density, lower specific surface area (which minimizes side reactions), and higher volumetric capacity compared to nanometer-sized particles.[31] Then, the silicon particles along with dispersant and photo-initiator are mixed with UV-curable resin by an open-source bottle roller.[32] The slurry was then used to print an acrylate–silicon composite using an SLA 3D printer. After pyrolysis in an N_2 atmosphere, the anodes were assembled into coin cells in a glove box. The materials were characterized at each step using spectrometry analysis, differential thermal analysis (DTA), and thermogravimetric analysis (TGA) of the polymer resin, optical microscopy on the printed parts, as well as scanning electron microscopy (SEM), energy-dispersive X-ray spectroscopy (EDS), X-ray diffraction (XRD) on the pyrolyzed parts before and after cycling, and Raman spectra on the pure transparent red resin before and after pyrolysis. Additionally, electrochemical characterizations, including cyclic voltammetry, galvanostatic charge–discharge, and electrochemical impedance spectroscopy (EIS), were performed on the assembled batteries.

2 Results and discussion

2.1 UV-vis spectrometry

The absorbance results for the silicon-based resins indicate that adding solid content leads to an increase in resin absorbance index which means more energy is required to start the polymerization (Fig. 1A). Due to the dark colour, Si powder is known for its high optical absorbance and refractive index. This high optical absorbance of Si means that sufficient light does not reach deeper parts of the slurry to initiate photopolymerization.[33] This significantly reduces the penetration depth and curing thickness of the printed part.[33] It is also noticeable that adding carbon black to the resin while having the same solid load increases the absorbance of the resin compared to when the resin only contains silicon which is because carbon black is darker in colour. As a result, the amount of solid load in the resin is more limited. Also, to achieve effective curing, a photoinitiator, which has high initiating activity and a broad absorption wavelength range is required.[33] Also, spectrometry analysis of different polymer resins from various manufacturers reveals that the colorbase resin from 3DRS, which is transparent, exhibits the lowest absorbance index (Fig. 1B). Following this, the Prusament transparent red resin also shows a relatively low absorbance index. Thus, the colorbase and transparent red resins are identified as the most suitable candidates.

2.2 DTA and TGA

The DTA results show the decomposition of various elements at different temperatures (Fig. 2A). The peaks observed up to 600 °C are attributed to the decomposition of organic compounds of H_2O, CO, CO_2, CH_4, and H_2, as well as the polymer burnout. This stage of decomposition results in significant weight loss, which leaves the free carbon residue behind. The TGA curves reveal that the Prusament transparent red resin exhibits less weight loss compared to the other tested resins (Fig. 2B). This indicates a higher carbon content in this resin which means
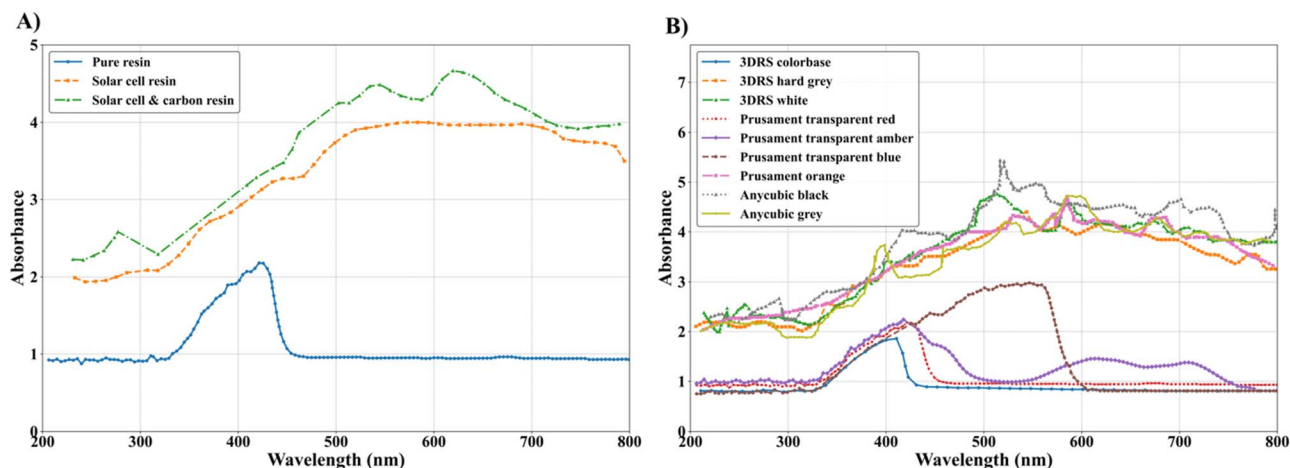
Fig. 1 UV-vis spectrometry results of the (A) resins with solid load, and (B) pure acrylate resins.

that after pyrolysis it shows less shrinkage. This characteristic is beneficial for anode fabrication where mechanical integrity and strength are important. Considering the TGA results along with the UV-vis spectrometry, the best candidate for customizing the resin is the transparent red resin, as it offers a low absorbance index and the highest carbon content.

2.3 Raman spectra and XRD

Fig. 3A shows the Raman spectra of the pure transparent red resin before and after pyrolysis. Before pyrolysis, the spectrum exhibits peaks at 1287, 1414, 1616, 1641, 1700, 1725, 2881, and 2947 cm^{-1}, which are corresponding to various functional groups characteristic of the polymeric structure. The peaks in the 1700–1725 cm^{-1} range indicate the presence of carbonyl groups. Also, peaks at 2881 and 2947 cm^{-1} are related to C–H stretching in aliphatic and aromatic structures. The bands at lower wavenumbers suggest C=C and C–O stretching modes, which are consistent with the acrylate-based resin composition.[34–36] After pyrolysis, the spectrum shows only two dominant peaks at 1607 and 1373 cm^{-1}. These correspond to the G-band and D-band, respectively, which are characteristic of

graphitic carbon. The disappearance of peaks associated with oxygen-containing and aliphatic groups confirms the decomposition of the organic matrix, which leaves behind a disordered carbonaceous structure. The presence of the D-band explains the formation of defective or amorphous carbon, while the G-band indicates the development of graphitic domains.[37] These results confirm that pyrolysis effectively removes non-carbon elements and converts the resin into a partially graphitized material with residual disorder. Additionally, a broad peak appears between 2600 and 3000 cm^{-1}, which corresponds to the 2D band of graphitic carbon.[38] In the initial pyrolysis run, the 3D-printed anode samples were heated to 1400 °C. In the XRD results shown in Fig. 3B, the peaks at 36.18°, 60.49°, and 72.24° are attributed to the SiC phase (reference code 01-073-1708). These peaks correspond to the characteristic diffraction angles of SiC, specifically the (111), (220), and (311) crystallographic planes, respectively. This XRD analysis shows that the reaction between silicon and carbon at high temperatures led to SiC formation. In addition to the primary peaks, several minor diffraction peaks are observed in the as-prepared sample, which likely result from interactions among impurities during high-
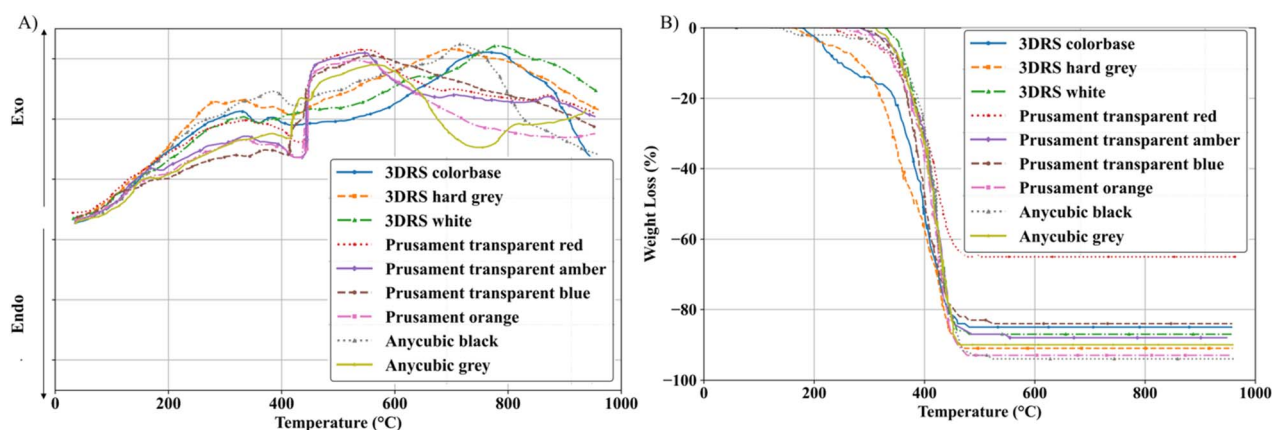

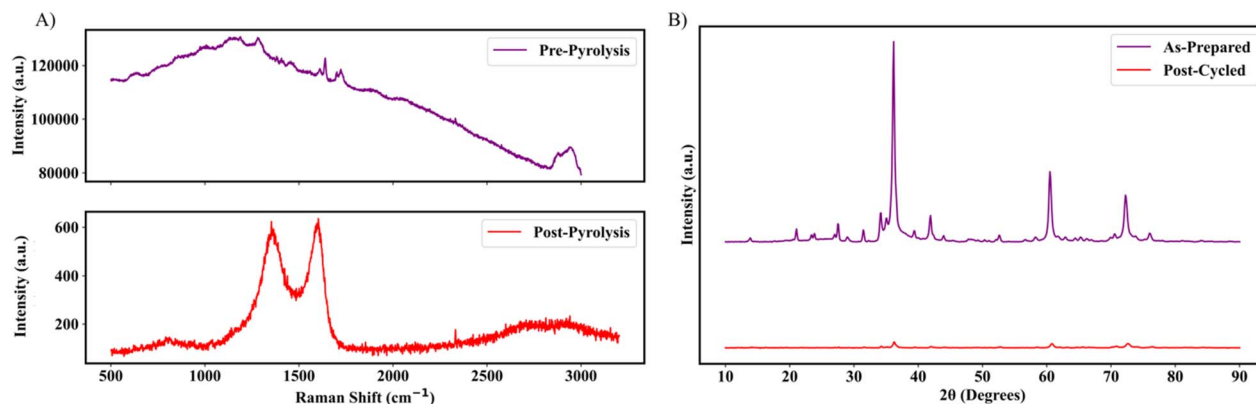Fig. 2 (A) DTA, and (B) TGA results from different acrylate resins.

Fig. 3 (A) Raman spectra of the pure transparent red resin before and after pyrolysis, and (B) XRD result of samples pyrolyzed at 1400 °C.

temperature processing. For instance, the small peaks at 27.55°, 66.23°, and 70.58° are attributed to SiO_2 (silicon dioxide) (reference code: 01-086-1564). This finding aligns with the EDS analysis of the acid-washed samples, where residual oxygen was detected. The presence of SiO_2 may arise from partial oxidation of silicon during pyrolysis or from residual silicon oxides that were present in the original material prior to thermal treatment. Additionally, peaks at 34.16° and 65.31° are related to FeO (iron(II) oxide) (reference code: 96-900-9771), which is supported by EDS results showing traces of residual Fe after acid washing. Additionally, post-cycling XRD analysis revealed a change in the silicon crystal size. Initially, using the Scherrer formula, the average size of silicon crystallite was measured to be 249 Å, but after cycling, it decreased to 163 Å. The reduction in crystal size suggests that the silicon experienced stress-induced fracturing during the lithiation/delithiation process, which is a well-known limitation of silicon-based anodes. Despite this structural degradation, the carbon matrix played a key role in buffering the mechanical strain, accommodating the volume changes, and preventing structural collapse. This is supported by the battery cycling performance, which demonstrates that the carbon network effectively mitigated cracking and maintained electrode integrity over extended charge–discharge cycles.

Furthermore, post-cycling XRD analysis indicates a noticeable reduction in peak intensities. This decrease can be attributed to the formation of amorphous lithium silicate (Li_xSiO_y) and lithium silicide (Li_xSi) phases.[38] Additionally, the incorporation of lithium into the silicon structure disrupts its original crystalline arrangement, which further contributes to the peak intensity reduction.

2.4 Optical microscopy and visual inspection

Optical microscope analysis of the printed samples (Fig. 4A) taken by the Openflexure microscope revealed that the first cured depth, printed with the polymer resin, increased from the 0.03 mm set in the slicer to 0.4 mm. This increase is attributed to the increase in the exposure time for the first layer to ensure the resin was fully cured and adhered to the build platform. Conversely, the cured thickness of the silicon resin reduced

from 0.03 mm to 0.016 mm which is due to the absorbance of the light by the powder which was shown by the UV-vis spectrometry. Also, the CAD model of the designed anode, along with the dimensions of the printed and pyrolyzed parts, are shown in Fig. S2.† The anode was designed with an initial diameter of 18.5 mm and a thickness of 0.9 mm. The printed part retained a diameter of 18.5 mm, which was consistent with the CAD design. The thickness of the as-printed part was measured at 0.5 mm, which corresponds to the silicon resin layer after the polymer resin was removed. During pyrolysis, the anode experienced dimensional shrinkage due to the removal of organic components and structural densification. The diameter decreased to 9 mm, which corresponds to a shrinkage of 51%, while the thickness reduced to 0.4 mm, which corresponds to a shrinkage of 20%.

2.5 SEM and EDX

The SEM images of the as ball milled and acid washed solar cell powder are shown in Fig. S3.† As can be seen in Fig. S3A and B,† silicon (Si), carbon (C), oxygen (O), silver (Ag), aluminium (Al), tin (Sn), lead (Pb), and iron (Fe) coexist within the powder. Following the acid wash with HCl (Fig. S3C and S3D†), the composition is altered, with only Si, C, O, and Fe remaining in the powder. During the acid washing process, Al is converted into soluble aluminium chloride ($AlCl_3$), Sn into tin chloride ($SnCl_2$), and Ag into silver chloride (AgCl). Si remains intact because it reacts with HCl only at elevated temperatures (above 350 °C). SEM images of the 3D printed samples after pyrolysis (Fig. 4B) revealed the formation of distinct carbon residue and silicon carbide (SiC) domains which support the XRD finding. The EDX analysis shown in Fig. 4C further confirmed the presence of these phases, which shows clear signals corresponding to carbon and silicon. At this elevated temperature, silicon from the solar cell waste reacted with carbon residue from the acrylate resin and led to the formation of SiC. The generation of SiC is undesirable for lithium-ion battery anodes due to its electrochemical inactivity and non-conductive nature. While silicon has a high capacity for lithium storage, the formation of SiC reduces the amount of active silicon available for the (de)lithiation process. This limits the overall charge
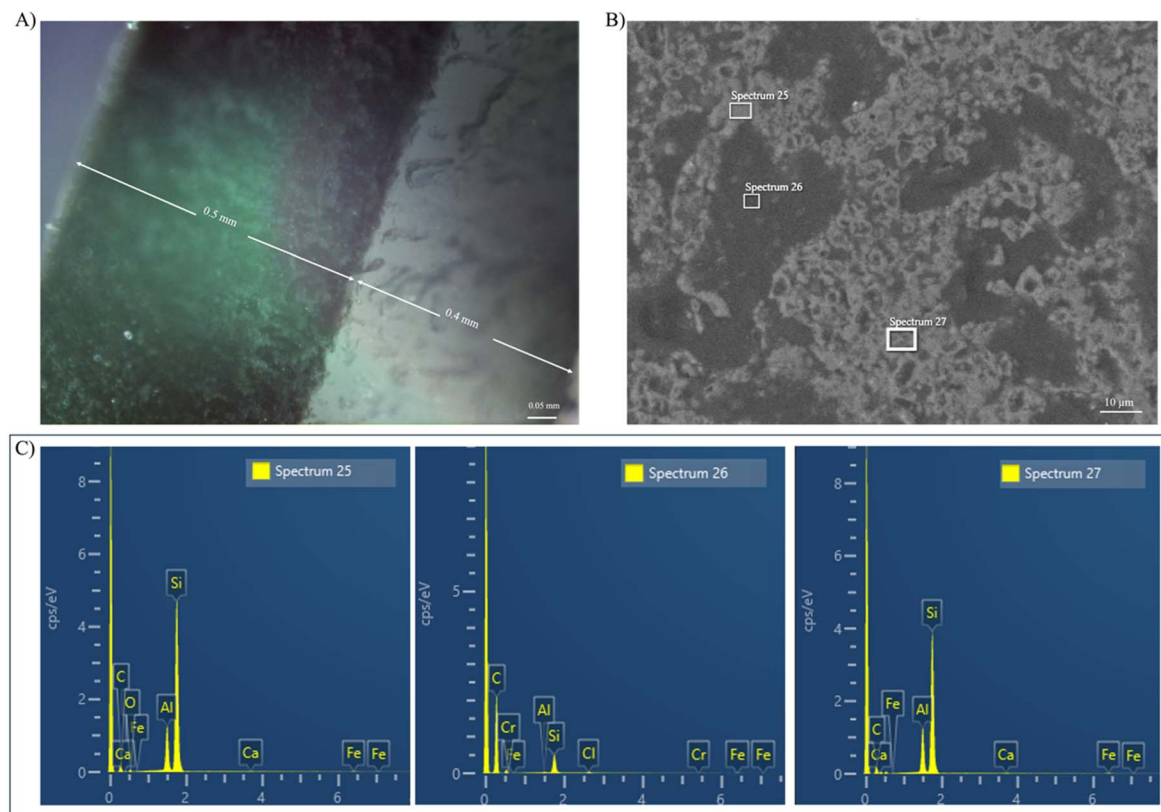
Fig. 4   (A) Optical microscopy image of printed sample using openflexure microscope, (B) SEM, and (C) EDX of the pyrolyzed samples at 1400 °C.

storage capacity of the anode and a reduction in the specific capacity observed during electrochemical testing could be attributed to the formation of this component. Moreover, the relatively low electrical conductivity of SiC, which arises from its wide bandgap and the scarcity of free charge carriers,[39] disrupts electron conduction pathways and prevents Li-ion diffusion. In addition, SiC tends to nucleate or accumulate at grain boundaries during high-temperature processing, since these regions have higher defect densities and localized stress that facilitate the reaction between silicon and carbon. As a result, SiC clusters can create localized resistive regions, which makes the charge transport more difficult and adversely affects both rate capability and long-term cycling stability. These factors lead to decreased charge-transfer efficiency and reduced overall battery performance. To achieve better performance, the formation of conductive carbon network surrounding the silicon particles is desirable. This carbon structure would improve electrical conductivity and buffer the expansion of silicon during lithiation which preserves the structural integrity of the anode.

2.6   Cyclic voltammetry

Fig. 5A displays the cyclic voltammetry (CV) profile of the anode material. As confirmed by EDS, the structure contains both silicon and oxygen, and as shown by the XRD results, crystalline silicon oxide is present. The reduction peak at 0.9 V is attributed to the irreversible conversion of surface silicon oxide into Li_x-SiO_y,[40–42] which is a reaction that also contributes to the

formation of the SEI. Although this process results in some initial capacity loss, it introduces a buffering matrix that helps accommodate the significant volume expansion during lithiation. Following this, the reduction peak at 0.46 V corresponds to the reversible lithiation of the silicon phase, which leads to the formation of a lithium–silicon alloy. Notably, given the confirmed presence of oxygen in the structure, this reversible reaction involves not only the formation of pure lithium silicide but also oxygen-modified lithiated silicon species, which could further enhance the capacity of the anode. In the delithiation sweep, the peak at 0.25 V indicates Li–Si dealloying, while the peak at 0.86 V likely reflects the evolution or partial decomposition of the SEI, which suggests ongoing changes in the organic and inorganic SEI components over cycles. This behavior suggests a stable and reversible lithiation–delithiation process, with minimal degradation over the observed cycles. Additionally, the overlapping curves and the slight increase in intensity at 0.25 V across cycles imply high reversibility, which shows that the anode material maintains a consistent electrochemical response.

2.7   Charge discharge

The galvanostatic charge/discharge result is shown in Fig. 5B. The specific capacity at 1C began at approximately 400 mA h g^{-1}, with a coulombic efficiency exceeding 100% and 89% capacity retention over 200 cycles. These values are comparable to reports in the literature indicating
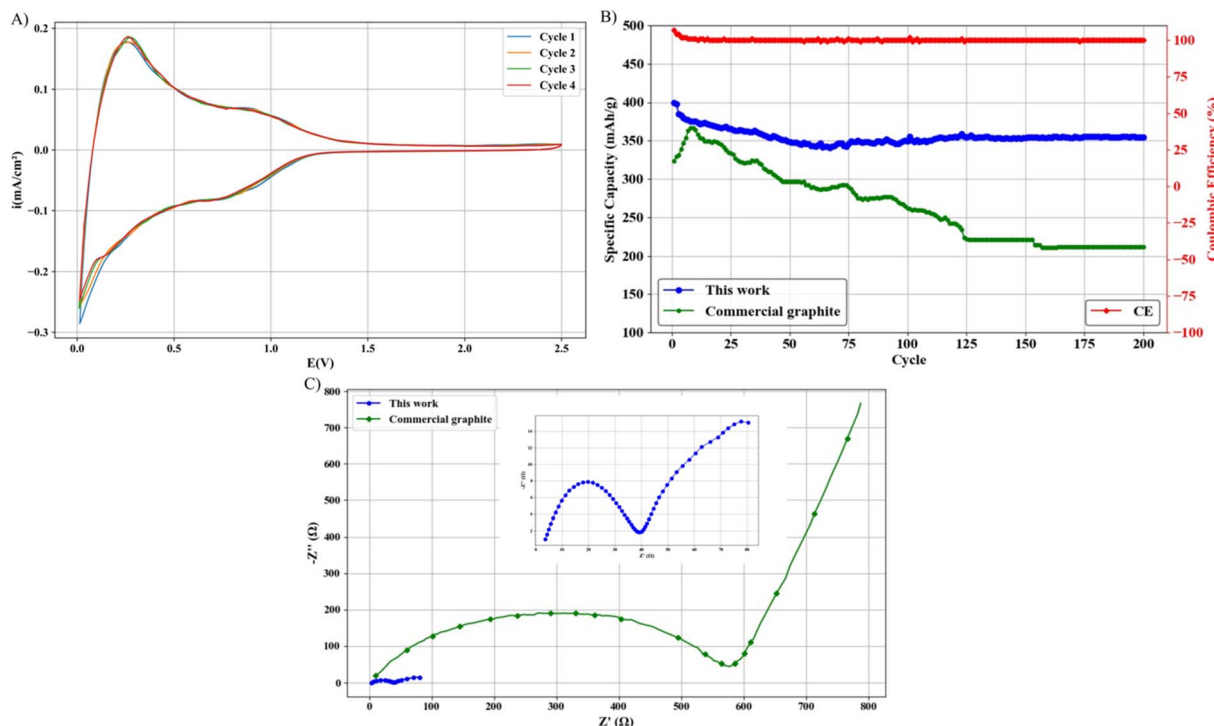
Fig. 5 (A) Cyclic voltammetry result, (B) Specific capacity result *vs.* commercial graphite anode, and (C) EIS spectra of the printed samples *vs.* commercial graphite anode.

426.78 mA h g^{-1} at a rate of 0.5 A g^{-1}, where 10% solar cells and 90% graphite were used as anodes through conventional methods.[14] Additionally, other studies have reported higher capacities, such as 306 mA h g^{-1} at a 1C rate when using 5% silicene and 95% graphite.[43] The specific capacity is also higher than the commercial graphite ($\sim$325 mA h g^{-1})[43] when cycled at 1C with the capacity retention of 66% over 200 cycles. Despite the relatively low percentage of active material (12%) in the samples, the performance remains comparable to traditional methods which highlights the potential of this approach.

It is expected that increasing the solid load will further enhance efficiency by increasing the availability of active silicon for lithium storage, which would, in turn, raise the specific capacity. Also, as confirmed earlier by SEM and XRD results, the reduced specific capacity observed may be linked to the formation of SiC.

2.8 EIS

The EIS curve of the anode in Fig. 5C reveals a semi-circle in the high-frequency region with a low charge transfer resistance (R_{ct}) of 35.56 Ω, comparable to the 21.45 Ω reported in the similar work[14] and significantly lower than the 146 Ω observed in another work,[43] and commercial graphite ($\sim$577 Ω).[43] Additionally, the slight zero-point offset in the high-frequency region can be attributed to minimal resistance through the electrodes and low contact resistances within the cell components. This performance is likely due to three main factors. First, the conductive carbon network formed during pyrolysis facilitates efficient electron transport and rapid charge transfer at the

silicon-electrolyte boundary. This carbon can help maintain a stable interface, which minimizes typical issues in silicon anodes, including high internal resistance and volume expansion. Secondly, the meshed geometry produced by 3D printing creates interconnected pathways that support both electron conduction *via* the carbon framework and ionic diffusion within the silicon matrix. This design provides an efficient interface for charge transfer, which reduces internal resistance. An additional benefit of the meshed geometry is evident in the flatter Warburg tail, which shows enhanced diffusion properties. Also, one of the notable advantages of the 3D printed anode design is the absence of polymer binders. Traditional anode structures often incorporate polymers like polyvinylidene fluoride (PVDF)[44,45] or carboxymethyl cellulose (CMC)[46] to bind the active materials together and enhance mechanical integrity. These polymers can hinder ionic conductivity and increase internal resistance, however, limiting overall electrochemical performance. In the binder-free approach, ionic pathways are less obstructed, which may contribute more efficient lithium-ion transport.

The results presented earlier show that for 3D printing the anodes with solar cell waste using an SLA printer, the initial step involves selecting the appropriate polymer resin. The absorbance index increases with the addition of solid load to the polymer resin, which subsequently reduces the penetration depth of light and decreases curing thickness. Therefore, resins with minimal absorbance index peaks are preferred. Another critical factor in resin selection is carbon content. In this regard, higher carbon content results in reduced shrinkage in the final

part. Based on these considerations, the Prusament transparent red resin with 47% carbon content was chosen. Printing the customized resin posed challenges, as the resin with solar cell waste did not adhere to the build plate.

To address this, multimaterial printing was employed. Initially, a polymer resin without solid load was used for the first layer. Subsequently, printing was paused, and the vat was changed to one containing the customized resin. However, this approach led to a new issue which was the separation of the polymer resin and the customized resin. This separation is critical because during pyrolysis, layers printed with polymer resin experience greater shrinkage which result in warping and non-uniformity in the anode structure. To address this, a flexible resin was used for the initial layer. The flexible resin has lower surface energy compared to the acrylate resin which results in inadequate interfacial contact. Additionally, the elastic nature of the flexible resin contrasts with the rigidity and denser network of the acrylate resin which causes internal stresses that induce delamination. Variations in photoinitiators and cure rates further contribute to incomplete or improper bonding at the interface. All these factors, help in the separation of the layers printed by the customized resin from the layers printed by the polymer resin. This is similar to the substrate release mechanisms used in metal 3D printing.[47,48]

After pyrolysis in a nitrogen atmosphere, the anodes were assembled into half cells and the electrochemical results demonstrate that SLA printing using solar cell waste is a promising method for producing lithium-ion battery anodes. These anodes showed 400 mA h g^{-1} specific capacity with 89% capacity retention and achieved more than 100% coulombic efficiency over 200 cycles. This capacity is approximately 94% of that reported in similar literature, where a specific capacity of 426.78 mA h g^{-1}, 87.5% capacity retention, and 100% coulombic efficiency over 200 cycles was achieved using an anode composed of 10% solar cells and 90% graphite *via* conventional methods e.[14] Additionally, the 3D printed anodes showed a 30.7% improvement in specific capacity compared to another study, which reported 306 mA h g^{-1}, over 93% capacity retention, and 97% coulombic efficiency for 500 cycles with an anode made from 5% silicene and 95% graphite.[43] Also, the anode fabricated in this work shows higher specific capacity than the commercial graphite ($\sim$325 mA h g^{-1}).[43] The notable advantage of this work, however, lies in the fact that no graphite was used in the fabrication of these anodes. The absence of graphite not only simplifies the process but also reduces dependency on this commonly used carbon source which makes the approach more sustainable and offers flexibility in tailoring the material composition.

Moreover, the choice of acrylate resin as a carbon source, compared to graphite, presents additional sustainability benefits. Unlike graphite, which requires energy-intensive mining and purification processes that have environmental impacts such as deforestation and water consumption,[49–52] acrylate resin can be sourced from industrial byproducts or bio-based feedstocks.[53–56] This makes it a more environmentally friendly alternative. Moreover, acrylate resin is highly customizable,[57] which allows for chemical modifications, such as introducing functional groups like carboxyl or hydroxyl groups to enhance the binding of the resin with silicon particles,[58] that can improve the performance of the anode and structure. The use of acrylate resin, especially in combination with solar cell waste, also aligns with a circular economy approach[59] which repurposes waste materials and potentially lowering the overall carbon footprint of the anode production process.

This battery performance in this work is attributed to the residual carbon effect[60] from the pyrolysis of the polymer resin, which buffers volume changes in silicon atoms during cycling. The carbon also enhances conductivity within the anode and increases accessibility to active sites, contributing to overall battery efficiency and stability.[60] So far in this work, the fabrication of anodes for lithium-ion batteries using solar cell waste through SLA printing has been successfully developed which demonstrated stable battery performance. The observed electrochemical performance metrics, with a specific capacity higher than that of commercial graphite-based batteries (372 mA h g^{-1}), suggest that the approach is promising and can be further optimized. This method is an innovative recycling technique and is promising in integrating waste materials from the PV industry into battery production which addresses sustainability and recycling challenges. The vast amounts of generated solar cell waste could be repurposed which leads to substantial material savings and reduced environmental impact. By 2030, it is estimated that approximately 1.7–8 million tons of solar photovoltaic waste will be generated globally.[61] Each standard 250 W solar panel weighs around 19 kg and contains approximately 0.573 kg of silicon.[62] This means that 51 thousand tons of silicon will go to waste as solar panels reach the end of their life cycle by 2030. If the resin used for anode fabrication contained a solid load of 12% solar waste, approximately 0.0015 gr of solar waste would be incorporated into each coin cell, with each anode weighing 0.0125 g. Given the total amount of silicon waste, it can be calculated that approximately 34 billion batteries could be produced annually. By using the method introduced in this work for anode production, around 403.75 tons of graphite could be saved annually in the production of 34 billion batteries. This estimate is based on the assumption that each anode weighs 0.0125 g, and considering that commercial batteries typically use more than 95% graphite in the anode.[63] Therefore, by replacing graphite with silicon from solar waste, a significant graphite demand could be reduced annually.

The remaining challenge in this work is the low amount of solid load in the resin, which is limited due to the high absorbance index of the silicon powder. In other studies, increasing the Si/C loading has increased SEI resistance, which was primarily due to reduced accessibility of lithium ions to the active material caused by the conventional fabrication method.[64] In contrast, the porous electrode geometry in this work makes the silicon particles exposed to the electrolyte. This unique architecture allows lithium ions to diffuse more easily through the structure, even at higher solid loads. Moving forward, future work is needed to enhance the role of silicon and its high capacity in the battery by increasing the solid load in the polymer resin. This can involve modifying the chemical

composition of the customized resin as well as adjusting printer slicer parameters to optimize the ability to print high silicon loaded resins to improve performance and efficiency. It has been shown that increasing the active material loading in the anode leads to thicker electrodes, which allow more lithium ions to penetrate deeper into the structure. This makes it more difficult for the ions to return, however, which results in irreversible capacity loss and lower initial coulombic efficiency. By leveraging 3D printing, this challenge can be addressed by precisely controlling the electrode architecture, optimizing porosity, and enhancing ion transport pathways to improve electrochemical performance.[20] Also, since the current pyrolysis temperature has been shown to produce silicon carbide, which, as discussed, has reduced the battery performance, lower pyrolysis temperatures can be explored. Additionally, while the printed samples showed promising results, using advanced microstructures could further optimize their performance. The application of 3D printing in battery fabrication extends beyond geometric control. For instance, it enables the fabrication of complex and fine-grained microstructures, such as porous, hierarchical, and graded architectures,[65,66] which can enhance lithium-ion transport, optimize electrolyte accessibility, and improve mechanical stability. For instance, gyroid lattice structures offer a balance between high porosity and mechanical resilience, which can reduce the risk of cracking and create uniform stress distribution. Additionally, hierarchical designs,[67,68] which combine macro-scale porosity for efficient electrolyte flow with micro-scale features to maximize active surface area, have the potential to improve electrochemical performance. Furthermore, graded architectures,[69,70] which are characterized by gradual transitions in material density or pore size, can effectively buffer the mechanical stresses caused by the expansion and contraction of silicon during cycling, which enhance cycle life. Another avenue for improvement will be the utilization of pre-ceramic polymers, combined with solar cell waste, in a ratio with acrylate resin to further optimize the material properties and overall performance. Using pre-ceramic polymers presents several advantages, which include high structural stability and volumetric strain suppression.[71,72] By adding solar cell waste to this composition, an increased Si–Li alloying due to the higher silicon content and improved electrical conductivity is expected. Furthermore, while acid washing was performed to remove impurities from the recycled silicon powder, some residual contaminants remain, as identified in the XRD and EDS analyses. To further purify the material, alternative acid washing practices should be explored to effectively eliminate these impurities and improve the overall quality and consistency of the recycled silicon. Also, while the focus of this work was on demonstrating the feasibility of SLA 3D printing for fabricating anodes using solar cell waste, further electrochemical testing including rate performance is needed to comprehensively evaluate battery performance.

3 Conclusions

This study shows the potential of fabricating lithium-ion battery anodes using 3D printing with solar cell waste with a specific capacity of 400 mA h g^{-1} with 89% capacity retention and over 100% coulombic efficiency after 200 cycles. These results surpass the performance of commercial graphite-based anodes which offers a more sustainable approach. The role of acrylate resin as a carbon source and the recycling of solar waste aligns with circular economy principles which address both sustainability and material reuse challenges. Future work will focus on increasing the silicon solid load in the resin to increase the silicon role in the battery performance, optimizing the pyrolysis temperature to avoid forming SiC, and exploring advanced anode geometries to further enhance the performance and scalability of this method.

Data availability

The data supporting this study are available within the manuscript. Also, the experimental section is included in the ESI.†

Author contributions

Maryam Mottaghi: conceptualization, data curation, formal analysis, investigation, methodology, software, validation, visualization, writing – original draft, writing – review and editing, Apoorv Kulkarni: investigation, resources, methodology, writing – review and editing, Joshua M. Pearce: conceptualization, formal analysis, funding acquisition, methodology, project administration, resources, supervision, writing – original draft, writing – review and editing.

Conflicts of interest

There are no conflicts to declare.

Acknowledgements

References

1 J.-M. Tarascon and M. Armand, Issues and challenges facing rechargeable lithium batteries, *Nature*, 2001, **414**, 359–367.

2 B. Dunn, H. Kamath and J.-M. Tarascon, Electrical Energy Storage for the Grid: A Battery of Choices, *Science*, 2011, **334**, 928–935.

3 K. Liu, Y. Liu, D. Lin, A. Pei and Y. Cui, Materials for lithium-ion battery safety, *Sci. Adv.*, 2018, **4**, eaas9820.

4 B. A. Boukamp, G. C. Lesh and R. A. Huggins, All-Solid Lithium Electrodes with Mixed-Conductor Matrix, *J. Electrochem. Soc.*, 1981, **128**, 725–729.

5 H. Zhang, L. Wang, H. Li and X. He, Criterion for Identifying Anodes for Practically Accessible High-Energy-Density Lithium-Ion Batteries, *ACS Energy Lett.*, 2021, **6**, 3719–3724.

6 H. Arai, J. Garche, and L. Colmenares, in *Electrochemical Power Sources: Fundamentals, Systems, and Applications*, Elsevier, 2019, pp. 143–266.

7 M. R. Zamfir, H. T. Nguyen, E. Moyen, Y. H. Lee and D. Pribat, Silicon nanowires for Li-based battery anodes: a review, *J. Mater. Chem. A*, 2013, **1**, 9566.

8 K. Feng, M. Li, W. Liu, A. G. Kashkooli, X. Xiao, M. Cai and Z. Chen, Silicon-Based Anodes for Lithium-Ion Batteries: From Fundamentals to Practical Applications, *Small*, 2018, **14**, 1702737.

9 M. M. Rahman, S. Mateti, I. Sultana, C. Hou, A. Falin, P. Cizek, A. Glushenkov and Y. Chen, End-of-Life Photovoltaic Recycled Silicon: A Sustainable Circular Materials Source for Electronic Industries, *Adv. Energy Sustainability Res.*, 2021, **2**(11), 2100081.

10 J. M. Pearce, Photovoltaics — a path to sustainable futures, *Futures*, 2002, **34**, 663–674.

11 Md. S. Chowdhury, K. S. Rahman, T. Chowdhury, N. Nuthammachot, K. Techato, Md. Akhtaruzzaman, S. K. Tiong, K. Sopian and N. Amin, An overview of solar photovoltaic panels' end-of-life material recycling, *Energy Strategy Rev.*, 2020, **27**, 100431.

12 N. C. McDonald and J. M. Pearce, Producer responsibility and recycling solar photovoltaic modules, *Energy Policy*, 2010, **38**, 7041–7047.

13 H. F. Yu, M. Hasanuzzaman, N. A. Rahim, N. Amin and N. Nor Adzman, Global Challenges and Prospects of Photovoltaic Materials Disposal and Recycling: A Comprehensive Review, *Sustainability*, 2022, **14**, 8567.

14 Y. Boon Tay, Y. Sim, J. Ang Koon Keong, M. Iszaki Bin Patdillah, H. Min Chua, E. Tang, J. Jie, M. Srinivasan and N. Mathews, Upcycling End of Life Solar Panels to Lithium-Ion Batteries Via a Low Temperature Approach, *ChemSusChem*, 2022, **15**, e202200978.

15 A. Casimir, H. Zhang, O. Ogoke, J. C. Amine, J. Lu and G. Wu, Silicon-based anodes for lithium-ion batteries: Effectiveness of materials synthesis and electrode preparation, *Nano Energy*, 2016, **27**, 359–376.

16 J. Zhou and N. Lin, Synthetic Methodologies for Si-Containing Li-Storage Electrode Materials, *Adv. Energy Sustainability Res.*, 2022, **3**, 2100198.

17 L. Sun, Y. Liu, J. Wu, R. Shao, R. Jiang, Z. Tie and Z. Jin, A Review on Recent Advances for Boosting Initial Coulombic Efficiency of Silicon Anodic Lithium Ion batteries, *Small*, 2022, **18**, 2102894.

18 X. Huang, R. Guo, Y. Lin, Y. Cao and J. Wu, Si/SiC/C *in situ* composite microspindles as anode materials for lithium-ion batteries, *Electrochim. Acta*, 2022, **422**, 140546.

19 J. Smekens, R. Gopalakrishnan, N. Steen, N. Omar, O. Hegazy, A. Hubin and J. Van Mierlo, Influence of Electrode Density on the Performance of Li-Ion Batteries: Experimental and Simulation Results, *Energies*, 2016, **9**, 104.

20 Y. Liu, Z. Shu, Q. Wang, J. Wu, W. Lu, Q. Wang, A. Wang, Y. Ding and M. Ma, Understanding the effects of different loadings on properties of a silicon/carbon anode for lithium batteries, *RSC Adv.*, 2024, **14**, 38085–38093.

21 J. Wang, Q. Sun, X. Gao, C. Wang, W. Li, F. B. Holness, M. Zheng, R. Li, A. D. Price, X. Sun, T.-K. Sham and X. Sun, Toward High Areal Energy and Power Density Electrode for Li-Ion Batteries *via* Optimized 3D Printing Approach, *ACS Appl. Mater. Interfaces*, 2018, **10**, 39794–39801.

22 Z. Lyu, G. J. H. Lim, J. J. Koh, Y. Li, Y. Ma, J. Ding, J. Wang, Z. Hu, J. Wang, W. Chen and Y. Chen, Design and Manufacture of 3D-Printed Batteries, *Joule*, 2021, **5**, 89–114.

23 J. Ding, K. Shen, Z. Du, B. Li and S. Yang, 3D-Printed Hierarchical Porous Frameworks for Sodium Storage, *ACS Appl. Mater. Interfaces*, 2017, **9**, 41871–41877.

24 K. Shen, H. Mei, B. Li, J. Ding and S. Yang, 3D Printing Sulfur Copolymer-Graphene Architectures for Li-S Batteries, *Adv. Energy Mater.*, 2018, **8**, 1701527.

25 B. Li, X. Liang, G. Li, F. Shao, T. Xia, S. Xu, N. Hu, Y. Su, Z. Yang and Y. Zhang, Inkjet-Printed Ultrathin MoS_2-Based Electrodes for Flexible In-Plane Microsupercapacitors, *ACS Appl. Mater. Interfaces*, 2020, **12**, 39444–39454.

26 W. Zong, Y. Ouyang, Y.-E. Miao, T. Liu and F. Lai, Recent advances and perspectives of 3D printed micro-supercapacitors: from design to smart integrated devices, *Chem. Commun.*, 2022, **58**, 2075–2095.

27 M. Mottaghi and J. M. Pearce, A Review of 3D Printing Batteries, *Batteries*, 2024, **10**, 110.

28 J. M. Pearce, Building Research Equipment with Free, Open-Source Hardware, *Science*, 2012, **337**, 1303–1304.

29 A. Gibb, *Building Open Source Hardware: DIY Manufacturing for Hackers and Makers*, Addison-Wesley Professional, 2014.

30 M. Mottaghi, M. Rahman, A. Kulkarni and J. M. Pearce, AC/off-grid photovoltaic powered open-source ball mill, *HardwareX*, 2023, **14**, e00423.

31 L. Sun, Y. Liu, L. Wang, Z. Chen and Z. Jin, Stabilizing porous micro-sized silicon anodes *via* construction of tough composite interface networks for high-energy-density lithium-ion batteries, *Nano Res.*, 2024, **17**, 1–9.

32 M. Mottaghi, Y. Bai, A. Kulkarni and J. M. Pearce, Open source scientific bottle roller, *HardwareX*, 2023, **15**, e00445.

33 J. Tang, X. Guo, H. Chang, K. Hu, Z. Shen, W. Wang, M. Liu, Y. Wei, Z. Huang and Y. Yang, The preparation of SiC ceramic photosensitive slurry for rapid stereolithography, *J. Eur. Ceram. Soc.*, 2021, **41**, 7516–7524.

34 C. Miliani, M. Ombelli, A. Morresi and A. Romani, Spectroscopic study of acrylic resins in solid matrices, *Surf. Coat. Technol.*, 2002, **151–152**, 276–280.

35 C. Murli and Y. Song, Pressure-Induced Polymerization of Acrylic Acid: A Raman Spectroscopic Study, *J. Phys. Chem. B*, 2010, **114**, 9744–9750.

36 L. E. Eijsink, A. S. Sardjan, E. G. Sinnema, H. den Besten, K. J. van den Berg, J. Flapper, R. van Gemert, B. L. Feringa and W. R. Browne, In situ EPR and Raman spectroscopy in the curing of bis-methacrylate–styrene resins, *RSC Adv.*, 2022, **12**, 2537–2548.

37 P. Blyweert, V. Nicolas, J. Macutkevic, V. Fierro and A. Celzard, Tannin-Based Resins for 3D printing of Porous

Carbon Architectures, *ACS Sustainable Chem. Eng.*, 2022, **10**, 7702–7711.

38 D. B. Schuepfer, F. Badaczewski, J. M. Guerra-Castro, D. M. Hofmann, C. Heiliger, B. Smarsly and P. J. Klar, Assessing the structural properties of graphitic and non-graphitic carbons by Raman spectroscopy, *Carbon*, 2020, **161**, 359–372.

39 Q. Fang, S. Xu, X. Sha, D. Liu, X. Zhang, W. Li, S. Weng, X. Li, L. Chen, H. Li, B. Wang, Z. Wang and X. Wang, Interfacial degradation of silicon anodes in pouch cells, *Energy Environ. Sci.*, 2024, **17**, 6368–6376.

40 D. Garrido-Diez and I. Baraia, in *2017 IEEE International Workshop of Electronics, Control, Measurement, Signals and Their Application to Mechatronics (ECMSM)*, 2017, pp. 1–6.

41 L. Sun, X. Wang, Y. Liu, H. Xu, H. Wang, Y. Lu and Z. Jin, Facile Redox Synthesis and Surface Engineering of Porous Silicon from Zintl Compound for High-Performance Lithium Ion Battery Anodes, *ACS Appl. Mater. Interfaces*, 2024, **16**(39), 52349–52357.

42 J. Li, S. Yang, H. Zhou, L. Wang, Z. Yang, P. Meng, L. Hu and R. Hu, Facile synthesis of SiO2/C anode using PVC as carbon source for lithium-ion batteries, *J. Mater. Sci.: Mater. Electron.*, 2019, **30**, 69–78.

43 L. Sun, Y. Liu, L. Wang and Z. Jin, Advances and Future Prospects of Micro-Silicon Anodes for High-Energy-Density Lithium-Ion Batteries: A Comprehensive Review, *Adv. Funct. Mater.*, 2024, **34**, 2403032.

44 Y. Kanaphan, A. Klamchuen, V. Piyavarakorn, V. Harnchana, S. Srilomsak, J. Nash, T. Wutikhun, A. Treetong, M. Liangruksa and N. Meethong, Multilayer Silicene Nanosheets Derived from a Recycling Process Using End-of-Life Solar Cells Producing a Silicene/Graphite Composite for Anodes in Lithium-Ion Batteries, *ACS Sustainable Chem. Eng.*, 2023, **11**, 13545–13553.

45 H. Li, X. Huang, L. Chen, Z. Wu and Y. Liang, ChemInform Abstract: A High Capacity Nano-Si Composite Anode Material for Lithium Rechargeable Batteries, *ChemInform*, 2010, **31**(1), DOI: **10.1002/chin.200001017**.

46 L. Fransson, T. Eriksson, K. Edström, T. Gustafsson and J. O. Thomas, Influence of carbon black and binder on Li-ion batteries, *J. Power Sources*, 2001, **101**, 1–9.

47 N. Eshraghi, L. Berardo, A. Schrijnemakers, V. Delaval, M. Shaibani, M. Majumder, R. Cloots, B. Vertruyen, F. Boschini and A. Mahmoud, Recovery of nano-structured silicon from end-of-life photovoltaic wafers with value-added applications in lithium-ion battery, *ACS Sustainable Chem. Eng.*, 2020, **8**, 5868–5879.

48 A. S. Haselhuhn, E. J. Gooding, A. G. Glover, G. C. Anzalone, B. Wijnen, P. G. Sanders and J. M. Pearce, Substrate Release Mechanisms for Gas Metal Arc Weld 3D Aluminum Metal Printing, *3D Print. Addit. Manuf.*, 2014, **1**, 204–209.

49 A. S. Haselhuhn, B. Wijnen, G. C. Anzalone, P. G. Sanders and J. M. Pearce, In situ formation of substrate release mechanisms for gas metal arc weld metal 3-D printing, *J. Mater. Process. Technol.*, 2015, **226**, 50–59.

50 Climate-change impacts of graphite production higher than reported — study, **https://www.mining.com/climate-change-impacts-of-graphite-production-higher-than-previously-reported-study/**, accessed 1 November 2024.

51 P. Engels, F. Cerdas, T. Dettmer, C. Frey, J. Hentschel, C. Herrmann, T. Mirfabrikikar and M. Schueler, Life cycle assessment of natural graphite production for lithium-ion battery anodes based on industrial primary data, *J. Cleaner Prod.*, 2022, **336**, 130474.

52 A. D. Jara, A. Betemariam, G. Woldetinsae and J. Y. Kim, Purification, application and current market trend of natural graphite: A review, *Int. J. Min. Sci. Technol.*, 2019, **29**, 671–689.

53 R. Jacob Robin, Viability and Eco-Consequences of Synthetic and Natural Graphite for Lithium-Ion Battery Anodes in the USA, *IEEE Eng. Manag. Rev.*, 2024, **52**, 131–147.

54 J. Andreska and L. Hanel, Historical occurrence and extinction of Atlantic salmon in the River Elbe from the fourteenth to the twentieth centuries, *Arch. Pol. Fish.*, 2014, **23**(1), DOI: **10.1515/aopf-2015-0001**.

55 R. Pomilovskis, E. Kaulina, I. Mierina, A. Abolins, O. Kockova, A. Fridrihsone and M. Kirpluks, Wood pulp industry by-product valorization for acrylate synthesis and bio-based polymer development *via* Michael addition reaction, *J. Bioresour. Bioprod.*, 2023, **8**, 265–279.

56 C. Veith, F. Diot-Néant, S. A. Miller and F. Allais, Synthesis and polymerization of bio-based acrylates: a review, *Polym. Chem.*, 2020, **11**, 7452–7470.

57 S. Fattoruso, 3D printing of bio-based soybean oil epoxy acrylate resin, **https://webthesis.biblio.polito.it/27038/**, accessed 22 November 2024.

58 J. Borrello, P. Nasser, J. C. Iatridis and K. D. Costa, 3D printing a mechanically-tunable acrylate resin on a commercial DLP-SLA printer, *Addit. Manuf.*, 2018, **23**, 374–380.

59 W. Jiang, X. Jin, H. Li, S. Zhang, T. Zhou and H. Xie, Modification of nano-hybrid silicon acrylic resin with anticorrosion and hydrophobic properties, *Polym. Test.*, 2020, **82**, 106287.

60 J. Korhonen, A. Honkasalo and J. Seppälä, Circular Economy: The Concept and its Limitations, *Ecol. Econ.*, 2018, **143**, 37–46.

61 A. C. Martinez, E. M. Schiaffino, A. P. Aranzola, C. A. Fernandez, M.-L. Seol, C. G. Sherrard, J. Jones, W. H. Huddleston, D. A. Dornbusch, S. T. Sreenivasan, P. Cortes, E. MacDonald and A. Maurel, Multiprocess 3D printing of sodium-ion batteries *via* vat photopolymerization and direct ink writing, *JPhys Energy*, 2023, **5**, 045010.

62 K. Komoto, J.-S. Lee, G. Heath and A. Wade, *End-of-Life Management of Photovoltaic Panels: Trends in PV Module Recycling Technologies*, International Energy Agency Photovoltaic Power Systems Program (IEA PVPS), 2018.

63 D. Sah, Chitra and S. Kumar, Recovery and analysis of valuable materials from a discarded crystalline silicon solar module, *Sol. Energy Mater. Sol. Cells*, 2022, **246**, 111908.

64 European Carbon and Graphite Association (ECGA), Graphite in batteries, **https://ecga.net/wp-content/uploads/2023/02/Graphite-in-batteries_Infosheet_final.pdf**.

65 Y. Liu, Z. Shu, Q. Wang, J. Wu, W. Lu, Q. Wang, A. Wang, Y. Ding and M. Ma, Understanding the effects of different loadings on properties of a silicon/carbon anode for lithium batteries, *RSC Adv.*, 2024, **14**, 38085–38093.

66 N. Fonseca, S. V. Thummalapalli, S. Jambhulkar, D. Ravichandran, Y. Zhu, D. Patil, V. Thippanna, A. Ramanathan, W. Xu, S. Guo, H. Ko, M. Fagade, A. M. Kannan, Q. Nian, A. Asadi, G. Miquelard-Garnier, A. Dmochowska, M. K. Hassan, M. Al-Ejji, H. M. El-Dessouky, F. Stan and K. Song, 3D Printing-Enabled Design and Manufacturing Strategies for Batteries: A Review, *Small*, 2023, **19**, 2302718.

67 J. Du, Q. Cao, X. Tang, X. Xu, X. Long, J. Ding, C. Guan and W. Huang, 3D printing-assisted gyroidal graphite foam for advanced supercapacitors, *Chem. Eng. J.*, 2021, **416**, 127885.

68 Z. Guo and C. Zhou, Recent advances in ink-based additive manufacturing for porous structures, *Addit. Manuf.*, 2021, **48**, 102405.

69 R. Wang, Y. Zhang, W. Xi, J. Zhang, Y. Gong, B. He, H. Wang and J. Jin, 3D printing of hierarchically micro/nanostructured electrodes for high-performance rechargeable batteries, *Nanoscale*, 2023, **15**, 13932–13951.

70 G. Hyun, Y. Ham, J. Harding and S. Jeon, Towards optimal 3D battery electrode architecture: Integrating structural engineering with AI-driven optimization, *Energy Storage Mater.*, 2024, **69**, 103395.

71 W. Ji, H. Qu, X. Zhang, D. Zheng and D. Qu, Electrode Architecture Design to Promote Charge-Transport Kinetics in High-Loading and High-Energy Lithium-Based Batteries, *Small Methods*, 2021, **5**, 2100518.

72 S. S. Bishoyi, T. R. Mohanta and S. K. Behera, Preceramic polymer derived carbon encapsulated Si-C hybrids for lithium-ion battery anodes, *J. Alloys Compd.*, 2024, **1002**, 175267.